16th World Conference on Earthquake, 16WCEE 2017
Santiago Chile, January 9th to 13th 2017
Paper N° 3246 (Abstract ID)
Registration Code: S- G1460959662

Effects of shear-span-ratio and axial force on structural performance of CES columns with wing wall

S. Suzuki[(1)], H. Kuramoto[(2)]

[(1)] *Assistant Professor, Dept. of Architectural Eng., Osaka University, suzuki@arch.eng.osaka-u.ac.jp*
[(2)] *Professor, Dept. of Architectural Eng., Osaka University, kuramoto@arch.eng.osaka-u.ac.jp*
…

Abstract

A static analysis and static loading tests were conducted to investigate the effects of shear-span and axial force on structural performance of CES columns with wing wall in the one side. It was indicated through the analytical results that the shear-span length of column became about half of the column height when the column was subjected to compression in the bottom, while the shear-span length became about column height when the column was subjected to compression at wing wall in the bottom. In the experimental results, the shear failure of the wing wall tends to occur earlier, because significant shear cracks occurred in the wing wall. In addition, it was confirmed that the shear failure at wing wall in the top tended to occur in the loading direction when subjected to high compression axial force at column in the bottom.

Keywords: CES Column with wing wall in the one side, Non-liner analysis, Static loading tests, Shear-span, Axial force

1. Introduction

The authors have been conducting a continuous development study on a new composite structural system, Concrete Encased Steel (CES) structures composed of steel and fiber reinforced concrete (FRC), which has better seismic performance and construction workability than steel reinforced concrete (SRC) structures. Through experimental studies on CES columns, CES beam-column joints, a two-bay two-story CES frame and CES shear walls, it was confirmed that the CES members and frame have excellent structural performance [1]-[4].

In recent years, static loading tests were carried out on CES columns with wing wall in the one side, for which an embedded the longitudinal wall reinforcements were not anchored to beams. The variables investigated were the anchorage condition of steel at the edge of wing the wall. In the experimental results, the maximum capacities of specimens with or without anchorage of the steel at the edge of the wing wall were almost the same in the loading direction when subjected to compression at the wing wall in the bottom. On the other hand, shear cracks in the wing wall were decreased in the specimen without anchorage of the steel in the loading direction when subjected to tension at the wing wall in the bottom [5].

By the way, exterior columns were subjected to varying axial forces. In the previous studies on CES columns subjected to high compressive axial force, it was founded that the CES columns have good deformation capacities [6]. In case of a CES column with wing wall in the one side, however, the compressive failure of the wing wall may occur early. In addition, the shear-span length varies depending on the direction of the shear force, because the cross-sectional shape is asymmetry. However, studies on the effect of both varying axial force and shear-span for columns with wing wall in the one side can be found little.

In this study, static analysis and static loading tests were conducted to investigate the effects of shear-span and varying axial force levels on the structural performance of CES columns with wing wall in the one side.

2. Static analysis of a CES building consisting of columns with wing wall

2.1 Outlines of static analysis

The non-linear static analysis for a 5 story CES frame building with wing walls shown in Fig. 1 was conducted to determine the shear-span length and varying axial force level for the columns with wing wall in one side in the static loading test. Details of members in the 1st-story were shown in Fig. 2. The wing walls have the length of 2,000mm, the thickness of 200mm, and are longitudinal and transverse reinforcement ratios of 0.42%. In addition, the longitudinal wall reinforcements in the wing walls are not anchored to the beams.

The external force distribution applied is the *Ai* distribution. The horizontal load sequences consisted of two cycles for the inter-story drift angle of 0.25×10^{-2} rad., 0.5×10^{-2} rad., 0.75×10^{-2} rad., 1.0×10^{-2} rad. and 1.5×10^{-2} rad. were applied, respectively. The non-linear static analysis was conducted using the commercial software SNAP.

Multi-Spring (MS) model was employed for CES columns with wing wall in the one side. The mesh layout of MS model is shown in Fig. 3. MS model was composed of axial spring elements representing concrete and steel. The longitudinal wall reinforcements omitting the anchorage were ignored. The plastic hinge length of MS model is the same as the column depth, *D*, of 850mm.

For the skeleton curve of concrete subjected to compression, a non-linear model was adopted in the stress-rising region, and a bi-linear model was adopted in the stress-softening regions, as shown in Fig. 4(a). The degrading stiffness model was used as the hysteretic model. For the skeleton curve of steel, the bi-linear model was adopted when subjected to compression, while the tri-linear model was used to take into consideration of the bond behavior between concrete and steel when subjected to tension, as shown in Fig. 4(b). The skeleton curve of shear resistance in CES column with wing wall in the one side was expressed by the tri-linear model. The first point was expressed as shear cracking point. The strength Q_{cr} was calculated using Eq. (1). The second point was expressed as the ultimate strength point. The strength Q_{su} was calculated using the Eq. (2) [5]. The strain γ_u was assumed to be 0.004. The peak-oriented model was used for the hysteretic model, as shown in Fig. 5.

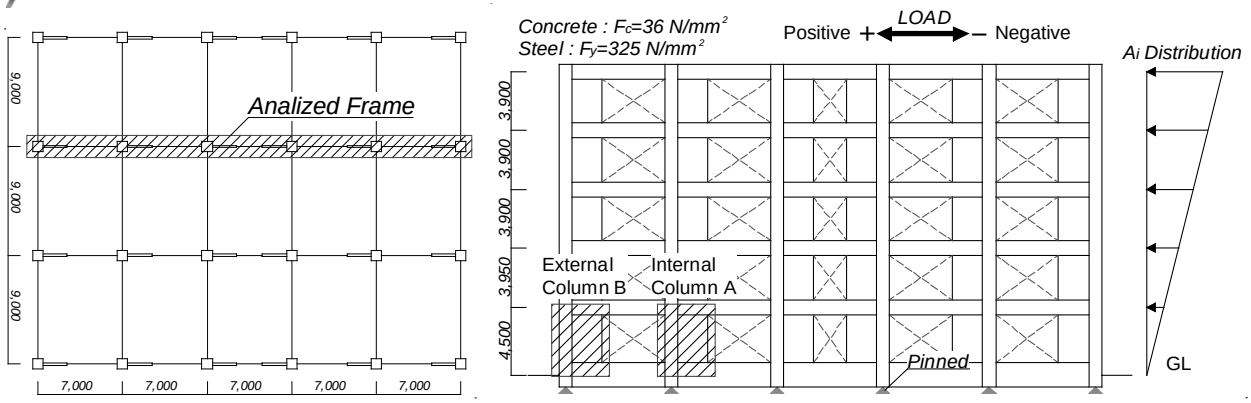

(a) Floor plan (1-story) (b) Elevation plan (Long side)

Fig. 1 - Analyzed building

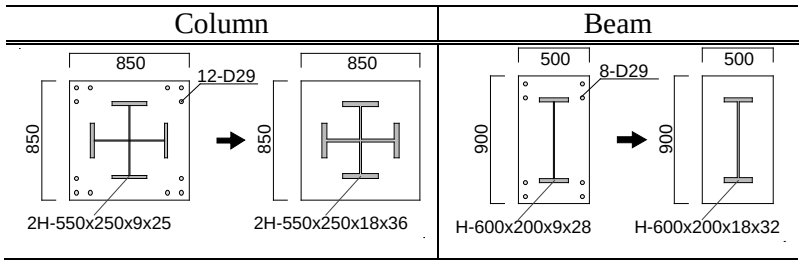

Fig. 2 - Cross-section of members (1-story)

However, it was confirmed that CES columns with wing wall did not reached the ultimate shear strength in the analytical result.

<Shear crack strength>

$$Q_{cr} = \sqrt{\sigma_{cr}\left(\sigma_{cr} + \sigma_0\right)} \cdot t_W \cdot l / \kappa_s \tag{1}$$

where σ_{cr} is cracking strength of concrete (=0.33$\sqrt{\sigma_B}$), σ_0 is axial stress at constant axial force, κ_s is shape coefficient (=1.5, assuming a rectangular cross-section), t_W is wall thickness, and l is wall length including column.

<Ultimate shear strength>

$$Q_{su} = {}_wQ_{su} + {}_cQ_{su} \tag{2}$$

$${}_cQ_{su} = \tan\theta_c \cdot (b - t_w) \cdot \mu \cdot D \cdot \sigma_B / 2 + \min\left({}_sM_u / h,\ \ t_w \cdot d_w \cdot \sigma_y / \sqrt{3}\right)$$

$${}_wQ_{su} = \tan\theta_w \cdot t_W \cdot l_{wa} \cdot \nu \cdot \sigma_B / 2$$

$$\mu = 0.5 + \left(b - b_f\right)/b \le 1.0,\ \nu = 0.74 - \sigma_B / 255$$

$$l_{wa} = l + A_{ce} / t_w,\ A_{ce} = A_c - N_{cc} / \sigma_B$$

$$\tan\theta_c = \sqrt{\left(2h/D\right)^2 + 1} - 2h/D,\ \tan\theta_w = \sqrt{\left(2h/l_{wa}\right)^2 + 1} - 2h/l_{wa}$$

where, b and D are the width and the depth of columns, ${}_sM_u$ is the flexural strength of steel in column, ${}_st_w$ and d_w are the thickness and depth of steel web in column, σ_y is the yielding stress of steel in column, b_f is the depth of steel flange in column, l is the length of wing wall, A_c is the section area of column.

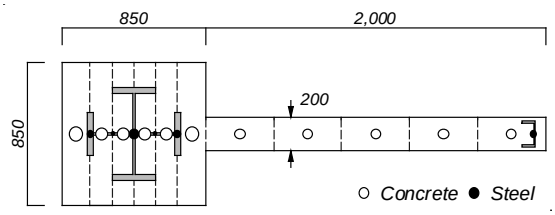

Fig. 3 - Messhing of MS model

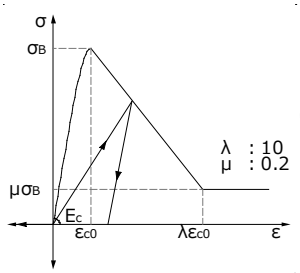

(a) Concrete

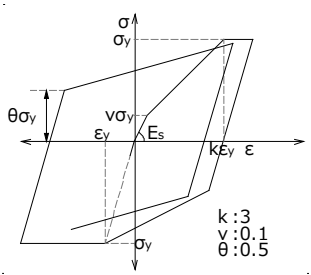

(b) Steel in column

Fig. 4 - Constitutive laws for materials[9)]

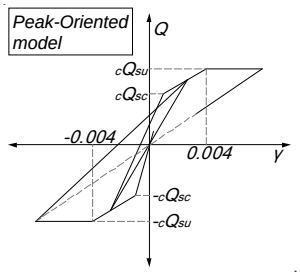

(a) Shear hysteretic modeling of column[9)]

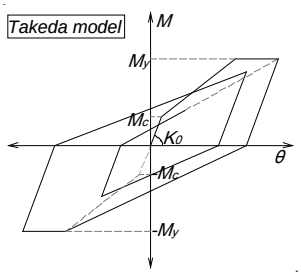

(b) Flexural hysteretic modeling of beam[3)]

Fig. 5 - Restoring force characteristics

The one component model was employed for CES beams using Takeda model for their hysteretic characteristics. The ultimate flexural strength M_u was calculated using the superposed strength method. the flexural crack strength M_{cr} was 1/3 of the ultimate flexural strength M_u. The stiffness reduction rate α_y after flexural crack was assumed to be 0.258.

2.2 Analytical results

The static analysis for the CES building was conducted focusing on the internal column A and external column B, as shown in Fig. 1(b). The base shear coefficient of the analyzed building was 0.538 when the inter-story drift angle at any story reaches 1.5 x 10^{-2} rad.

Axial force versus shear force relationships of the internal column A and external column B were shown in Fig. 7. The axial force level of the column A was constant regardless of shear force level. On the other hand, the axial force level of the column B was proportional to the shear force. The ratio of axial force to the shear force is approximately 2.5.

Shear-span ratio versus shear force relationships were shown in Fig. 8. Regardless of the direction of the shear force, the shear-span ratios of both internal and external columns were decreased with an increase of shear force. The value of shear-span ratio was about 1.0 in the cycle of 0.75 x 10^{-2} rad., when subjected to tensile axial force in the wing wall. The value of shear-span ratio was about 0.6 in the cycle of 0.75 x 10^{-2} rad, when subjected to compressive axial force in the wing wall. Because the longitudinal wall reinforcements of CES columns was not anchored to beams, the wing wall end did not contribute to bending moment when subjected to tension at the bottom. On the other hand, shear-span ratios of both columns when subjected to compression at the bottom were larger than those when subjected to tension at the bottom of wing wall because the wing wall contributed bending moment due to compression forces applying to the wing wall.

From the above results, the varying shear-span ratio depending on the loading directions and the loading method of axial force were adopted as the variables investigated in the static loading tests shown in Chapter 3. The shear-span ratio was 0.71 (shear-span length was 1,000mm) when subjected to tension at the bottom of wing wall, while the ratio was 1.42 (shear-span length was 2,000mm) when subjected to compression at the bottom of wing wall. On the other hand, the applied axial forces were the constant for the internal column A, while the varying axial force were applied for the external column B. However, the ratio of axial force to the shear force

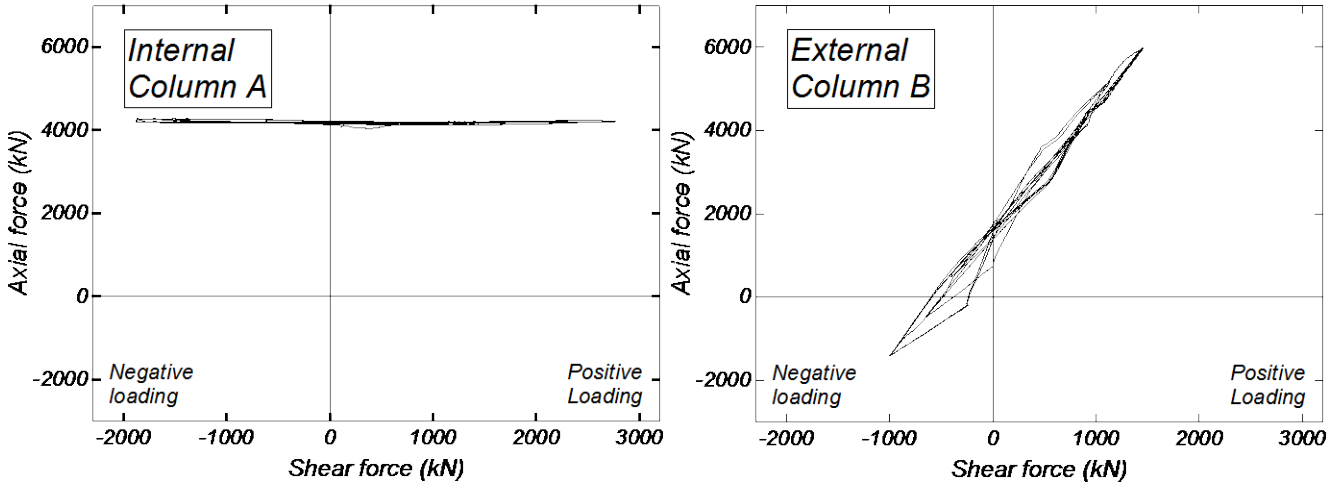

Fig. 7 - Axial force-shear force relationships in column

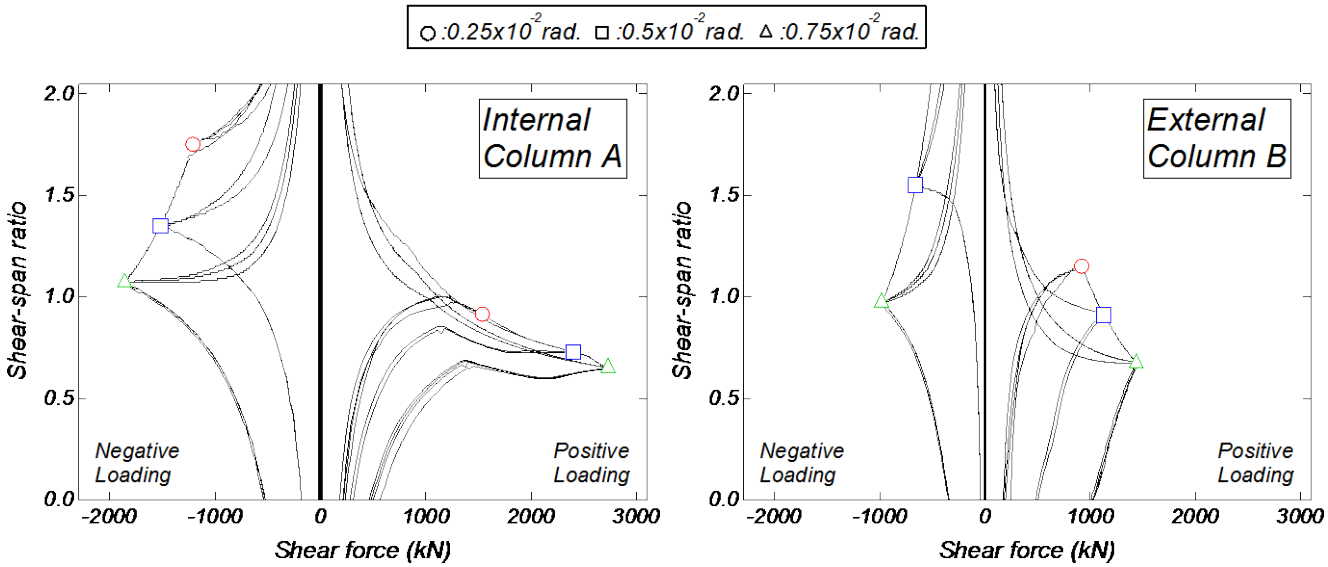

Fig. 8 - Shear-span ratio-shear force relationships in column

was limited to 1.3 due to the capacity of loading apparatus. The values of the ultimate flexural strength of CES columns with wing wall in the one side were varied with the variation of the ratio of axial force to shear force. However, the failure modes of the CES columns with wing wall in the one side were expected to be shear failure in the positive loading cycle and flexural yielding in the negative loading cycle. Therefore, it was judged that the effect of reduction of the ratio of axial force to shear force on the failure mode of CES columns with wing wall in the one side was small.

3. Test program

3.1 Description of Specimens

Three column specimens of 1/2-scaled were prepared, which were designed to simulate columns in the 1st story of a medium rise building. The configurations and bar arrangements of the specimens are shown in Figs. 9 and 10. Details of the cross-section are listed in Table 2. The columns had a 400mm square section with the height of 1,800mm. The wing wall had a section of 100 x 1000mm. The longitudinal wall reinforcement and the steel at

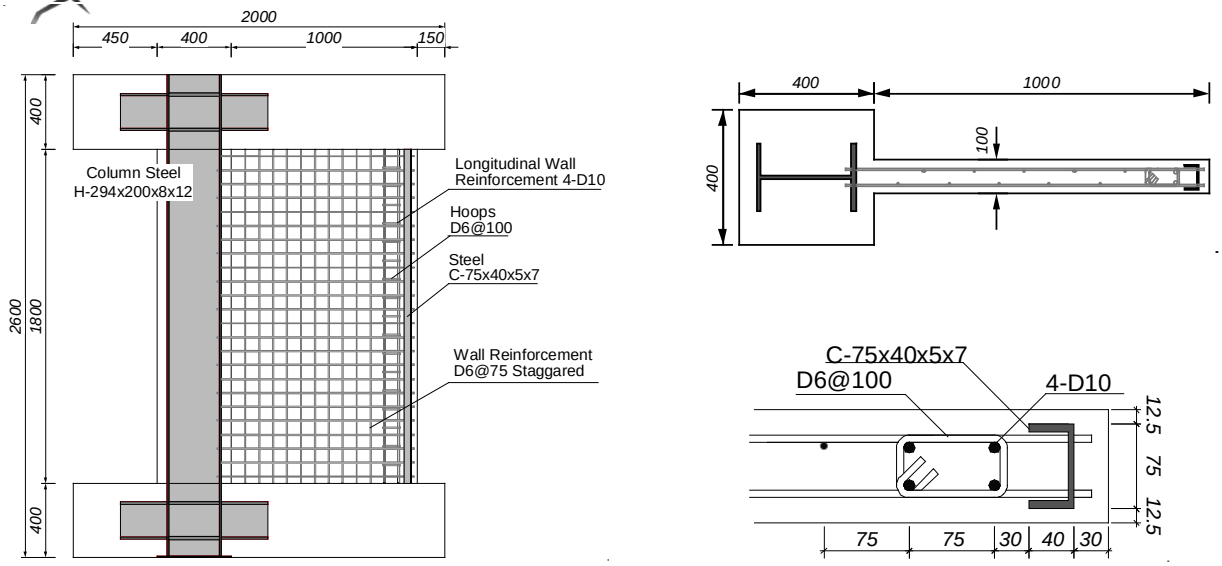

Fig. 9 - Configuration and bar arrangement of specimens

Table 3 - Material properties of FRC

Specimen	Compressive strength (N/mm^2)	Elastic modulus (kN/mm^2)	Strain at compressive strength (μ)
WWF1	55.1	29.5	2355
WWF4	50.7	29.7	2428
WWF5	54.7	31.0	2598

Table 4 - Material properties of steels and bars

Class	Specimen	Yield strength (N/mm^2)	Elastic modulus (kN/mm^2)	Tensile strength (N/mm^2)
PL-5	*WWF1*	328	206.5	451
	Others	331	198.4	442
PL-7	*WWF1*	314	205.1	448
	Others	336	195.5	428
PL-8	*WWF1*	328	201.9	469
	Others	333	205.7	436
PL-12	*WWF1*	306	201.3	467
	Others	295	203.3	407
D6	*WWF1*	320	163.3	483
	Others	320	163.3	458
D10	*WWF1*	367	183.2	500
	Others	352	170.5	439

Table 1 - Details of specimens

Column	B×D	400×400 (mm)
	Steel	H-294×200×8×12
Wing wall	Thickness	100 (mm)
	Length	1,000 (mm)
	longitudinal and transverse bars	D6@75 Staggered ($_wp$=0.42%)
Steel at edge of wing wall	longitudinal bars	4-D10
	steel	C-75×40×5×7
	hoops	D6@100

Table 2 - Experimental variables

		WWF1	*WWF4*	*WWF5*
Shear-span	Positive loading	2,000 (mm)	1,000 (mm)	
	Negative loading	2,000 (mm)		
Axial force	Loading method	Constant		Varying
	Ratio +:compression -:tension	+0.2		-0.02~ +0.35

the edge in a wing wall were not anchored to stubs (beams). The transverse wall reinforcements in a wing wall were securely fixed by welding them to the encased steel in the column.

The variables investigated were the shear-span length and applied axial force level. Specimens WWF1 and WWF4 were applied the constant axial force of 1,800kN and 1,700kN, respectively (axial force ratio of 0.2). On the other hand, the varying axial force was applied for Specimen WWF5 with the initial axial force of 850kN. The shear-span length in Specimen WWF1 was kept 2,000mm, while that in Specimens WWF4 and WWF5 was 1,000mm in the positive loading where the wing wall was subjected to tension at the bottom, and 2,000mm in the negative loading where the wing wall was subjected to compression at the bottom.

The mechanical properties of FRC and steel used are listed in Tables 3 and 4, respectively. Poly vinyl alcohol (PVA) fibers with the diameter of 0.66mm and the length of 30mm were used for the FRC. The volumetric ratio of the fibers was 1.0%.

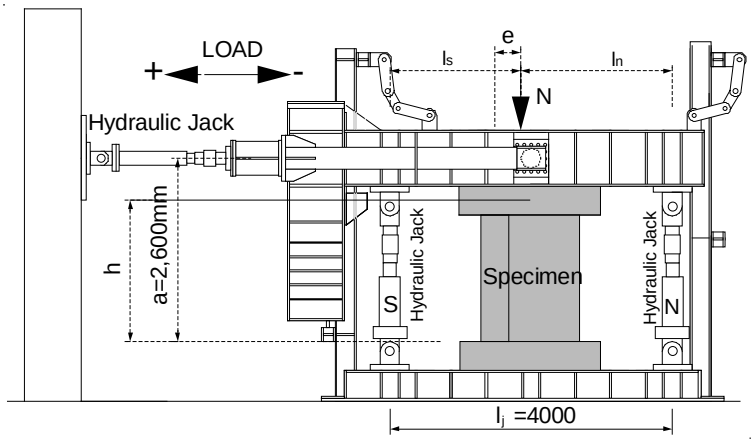

Fig. 10 - Loading apparatus

3.2 Loading Program

The loading apparatus used is shown in Fig. 10. The specimens were loaded horizontal cyclic shear forces using a hydraulic jack with a 2,000 kN capacity, while a axial force was applied by two vertical hydraulic jacks with a 2,000 kN capacity. During the testing, additional moment was also applied to the top of the specimen using the two vertical jacks to maintain the prescribed shear-span ratio, using the following equations.

$$N = \alpha \cdot Q + \beta \cdot N_0 \text{ (kN)} \tag{3}$$

$$N_0 = {}_cA \cdot {}_cr_u \cdot \sigma_B + {}_sA \cdot \sigma_y \text{ (kN)} \tag{4}$$

$${}_cr_u = 0.85 - 2.5\,{}_sp_c \tag{5}$$

$$N_n = l_s / l_j \cdot N + Q / l_j \cdot (h - a) \text{ (kN)} \tag{6}$$

$$N_s = l_n / l_j \cdot N - Q / l_j \cdot (h - a) \text{ (kN)} \tag{7}$$

where, α is the factor of varying axial force (WWF1 and WWF4 are 0, WWF5 is 1.3), Q is the applied shear force, β is the initial axial force ratio (WWF1 and WWF4 are 0.2, WWF5 is 0.1), N_0 is the axial strength including steel in column, ${}_cA$ is the cross-section area of concrete in column, ${}_sA$ is the cross-section area of steel in column, σ_B is the compressive strength of concrete, σ_y is the yielding stress of steel in column, ${}_cr_u$ is the reduction factor, ${}_sp_c$ is the steel ratio of column steel flange in compression, N_n and N_s are the axial force of north/south vertical hydraulic jacks, l_s and l_n are the distances from the position of north/south vertical hydraulic jacks to the center of gravity, l_j is the distance between vertical hydraulic jacks, h is the assumed height of applied shear force and a is the actual height of applied shear force.

The loading was conducted by controlling the relative drift angle, R, given by the ratio of the height corresponding to the measuring point for the horizontal displacement at the top of the specimen, h_0 (2,000mm), to the horizontal deformation, δ, i.e., $R=\delta/h_0$. The horizontal load sequences consisted of one cycle for R of 0.0625 x 10^{-2} rad. and 0.125 x 10^{-2} rad. respectively, and after R of 0.25 x 10^{-2} rad. two cycles for each relative drift angle were applied.

4. Experimental Results

4.1 Cracking Pattern

The cracking patterns at the loading cycle of 0.5 x 10^{-2} rad. and the final loading cycle of all specimens are shown in Fig. 5.

The compressive failure of concrete at the bottom of wing wall occurred in both Specimens WWF1 and WWF4. The damage process of these specimens is similar. However, the occurrence of compressive failure at

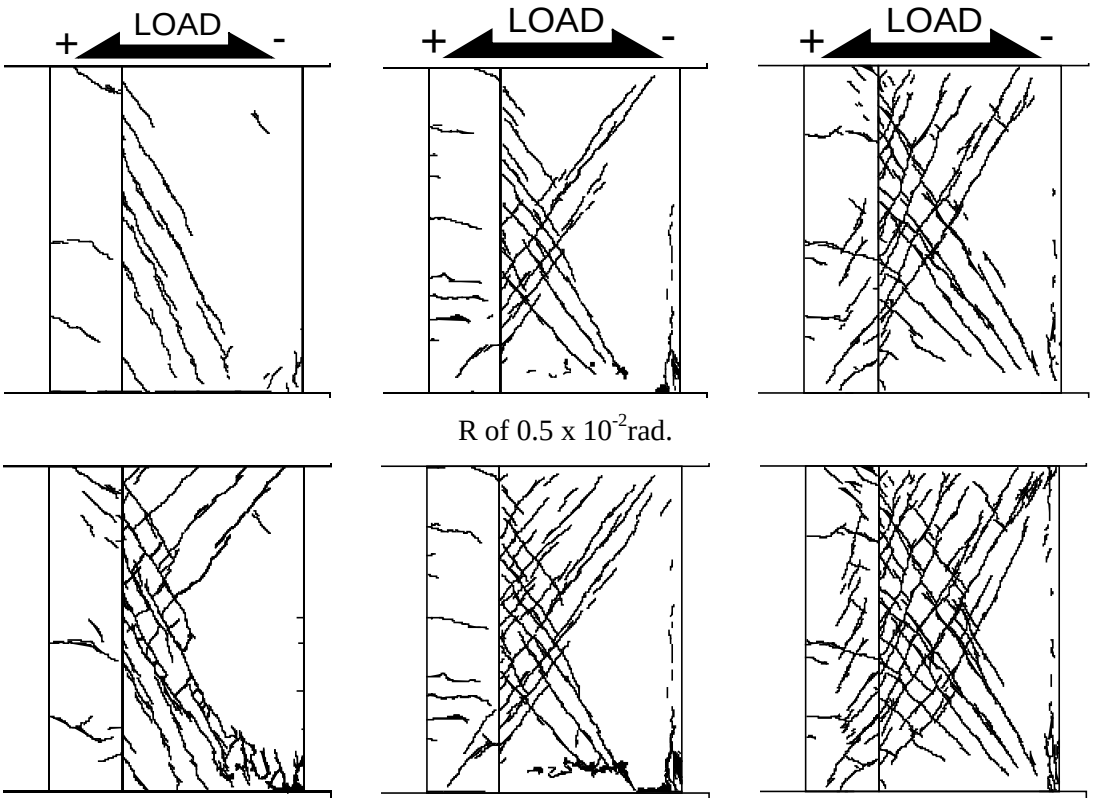

R of 0.5 x 10^{-2}rad.

Final loading cycle

Fig. 11 - Cracking patterns

the bottom of wing wall in Specimen WWF4 was earlier than that in Specimen WWF1. Moreover, the occurrence of shear cracks in the wing wall in the positive loading for Specimen WWF4 was more significant than that for Specimen WWF4. Therefore, the shear capacity of the wing wall in Specimen WWF4 deteriorated earlier in the negative loading than that in Specimen WWF1.

On the other hand, the shear cracks of the wing wall in Specimen WWF5 were more significant than that in Specimen WWF4 in the negative loading where the wing wall was subjected to compression at the bottom. However, the shear failure at the bottom of the wing wall in Specimen WWF5 did not occurred, as seen in Specimen WWF4. The shear failure of the wing wall occurred in the positive loading where the wing wall was subjected to tension at the bottom, because the wing wall was subjected to high compression at the top.

4.2 Shear force versus drift angle relationships

Shear force versus drift angle relationships are shown in Fig. 12. In the figure, circles, squares and triangles showed the points of the maximum capacities, the yielding of steel flange in column and the yielding of transverse wall reinforcement, respectively.

In Specimens WWF1 and WWF4, which were applied to the same constant axial force, the maximum capacities of Specimen WWF4 was about twice of Specimen WWF1 in the positive loading, because of the difference of shear-span ratio. Hysteretic characteristics of both specimens in the positive loading were S-shaped loop after stiffness degradation with flexural cracks at the bottom of wing wall, because of the omitting anchorage of longitudinal wall reinforcements. The quantity of absorbed energy in Specimen WWF4 was slightly larger than that in Specimen WWF1, because the occurrence of shear cracks in wing wall for Specimen WWF4 was significant, as shown in Fig. 11.

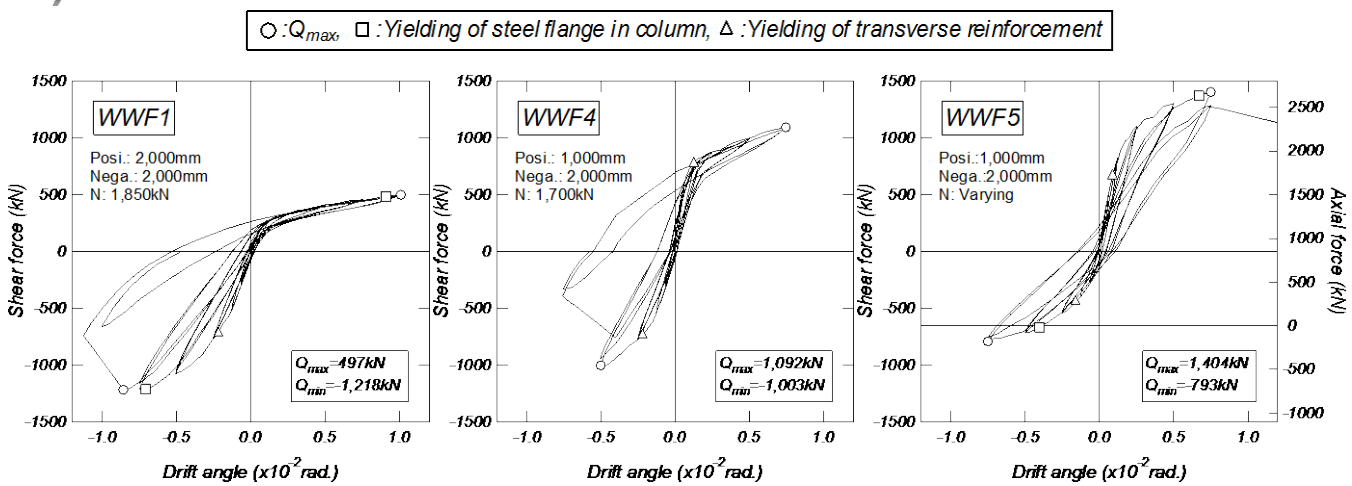

Fig. 12 - Shear force-drift angle relationships

On the other hand, the maximum capacities of both specimens in the negative loading were slightly different, regardless of the same shear-span ratio. It was thought that the shear transferring capacity of the wing wall in Specimen WWF4 was deteriorated, because the occurrence of shear cracks in Specimen WWF4 in the positive loading cycle just before that was more significant than that in Specimen WWF1, as described in the section 4.1. Hysteretic characteristics of both specimens in negative loading shaped stiffness degrading loop because of the effects of flexural cracks in the column and shear cracks in the wing wall.

In Specimens WWF4 and WWF5 with the different axial force levels, the maximum capacity of Specimen WWF5 was lower than that of Specimen WWF4 in the negative loading. On the other hand, the maximum capacity of Specimen WWF5 was higher than that of Specimen WWF4 in the positive loading. While the strength deterioration of Specimen WWF5 in the negative loading was not observed, that in positive loading was observed at R of 1.0 x 10^{-2}rad.

5. Evaluation of Ultimate Strength

The flexural strength Q_{mu} for CES columns with wing wall in the one side was calculated using the superposed strength theory, in which the tensile forces of the longitudinal wall reinforcement and the steel at edge of wing wall are omitted. The bending moments were calculated for the center of gravity for Specimen WWF1 and the plastic center of gravity for the other specimens.

The shear strength Q_{su} was calculated using Eq. (2). In the calculation of the shear strength of wing wall, the arch-mechanism was only considered because the anchorage of longitudinal wall reinforcement was omitted. On the other hand, the shear strength of CES column considered the arch-mechanism of concrete and flexural strength of steel.

The calculation results of the ultimate strength for all specimens are shown in Fig. 15 and Table 5, respectively. In the positive loading, the safety margin between the shear strength and the flexural strength for all specimen were larger than 1.0, and the failure modes were evaluated by the flexural yielding before shear failure. In Specimen WWF5, the flexural yielding of steel in CES column occurred before the shear failure of the wing wall occureed. Therefore, the failure mode in calculated results showed good agreement with that in test results. Moreover, the ratios of the maximum capacities to the flexural strength calculated by the superposed strength theory were 0.92 for Specimen WWF1, 1.13 for Specimen WWF4 and 1.10 for Specimen WWF5. Thus, good agreements were obtained between the maximum and calculated strengths.

In the positive loading, the safty margin between the shear strength and the flexural strength were 0.82 for Specimen WWF1 and 0.79 for Specimen WWF4. It was judged that the shear failure occurred in both specimens. These results are agree with the failure mode of the specimens in the experiment. However, the ratios of the

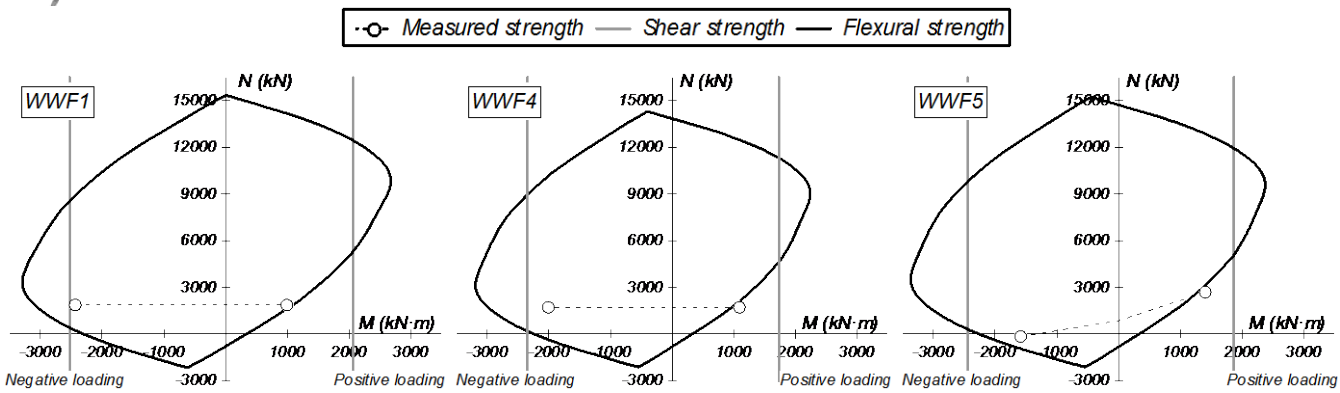

Fig. 13 - N-M interaction curves

Table. 5 - Measured and calculated strength

Unit: kN	WWF1		WWF4		WWF5	
	Positive loading	Negative loading	Positive loading	Negative loading	Positive loading	Negative loading
Measured strength Q_{exp}	497	1,218	1,092	1,003	1,404	793
Flexural strength Q_{mu}	543	1,544	967	1,492	1,279	1075
Shear strength Q_{su}	1,033	1,263	1,734	1,172	1,869	1,222
Q_{exp} / min(Q_{su}, Q_{mu})	0.92	0.96	1.13	0.86	1.10	0.74
Q_{su} /Q_{mu}	1.90	0.82	1.79	0.79	1.46	1.14

maximum capacity to the shear strength were 0.96 for Specimen WWF1 and 0.86 for Specimen WWF4. Calculated results of shear strength for these specimens were overestimated by the maximum capacity, because the shear cracks in the CES column did not occur until the maximum capacity. In addition, the shear capacity of wing wall in Specimen WWF4 was lower than that in Specimen WWF1, as shown in Section 4.1.

5. Conclusion

In this study, a nonlinear static analysis of a CES frame building with wing walls was conducted. The behaviour of CES columns with wing wall in the one side was examined focusing the variation of shear-span length and axial force. Moreover, static loading tests of CES columns with wing wall in the one side were conducted. From the analytical and experimental studies, the following conclusions can be drawn.

1) In the analytical results, the shear-span length of CES columns with wing wall in the one side became about half of the column height when subjected to tension in the bottom of wing wall. On the other hand, the shear-span length became about the column height when subjected to compression at the bottom of wing wall.

2) The shear failure of the wing wall occurred early in the loading direction when subjected to compression at the bottom of column, because significant shear cracks occurred at wing wall.

3) In CES columns with wing wall in the one side under high axial compression, the shear failure of the wing wall tends to occur in the loading direction when subjected to compression at the bottom of wing wall

4) Hysteretic characteristics of CES column with wing wall in the one side when subjected to tension at the bottom of wing wall were S-shaped loop, because the anchorage of longitudinal wall reinforcements was omitted. On the other hand, that when subjected to compression at the bottom of wing wall showed the stiffness degradation loop because of the effects of flexural cracks in the CES column and shear cracks in wing wall.

5) The ultimate flexural strength of CES columns with wing wall in the one side can be evaluated by the superposed strength theory. The ultimate shear strengths of the CES columns with wing wall were slightly overestimated by Eq. (2).

5. References

[1] Fujimoto T, Kuramoto H, and Matsui T (2008): Seismic performance of columns and beam-column joints in composite CES structural system, *Proceeding of the 14th World Conference on Earthquake Engineering*, Beijing, China.

[2] Fauzan, Kuramoto H, Matsui T and Taguchi T (2008): Test on 2-bay 2-story CES frame subjected to lateral load reversals, *Proceeding of the 14th World Conference on Earthquake Engineering*, Beijing, China.

[3] Matsui T, Kuramoto H (2008): Stress transferring mechanisms of composite CES beam-column joints subjected to seismic loading. *Proceeding of the 14th World Conference on Earthquake Engineering*, Beijing, China.

[4] Suzuki S, Matsui T and Kuramoto H (2012): A fundamental study on structural performance of CES shear walls with different anchorage condition of wall reinforcing bars, *Proceeding of The 15th World Conference on Earthquake Engineering*, Lisbon, Portugal.

[5] Mori S, Suzuki S, Koike S and Kuramoto H (2013): Structural performance of CES columns with one side wing wall under different anchorage conditions of the wall, *Proceedings of the Japan Concrete Institute*, 35 (2), 1165-1170, (in Japanese)

[6] Matsui T, Mizobuchi H and Kuramoto H (2010): FEM analysis and structural test of CES column with H-shaped steel, *Proceedings of the Japan Concrete Institute*, 32 (2), 1171-1176, (in Japanese)